Multiscale modelling of fluid and solute transport in soft tissues and microvessels

Yiling Lu and Wen Wang

Biofluids & Cell Mechanics Laboratory

Queen Mary, University of London

Running title: Transport in microvessels and soft tissues

Keywords: microcirculation, transport of solute and macromolecules, blood-wall interaction, transcapillary exchange, tissue oxygenation

Correspondence:

Professor Wen Wang

School of Engineering and Materials Science

Queen Mary, University of London

London E1 4NS

UK

Tel. +44 2078828871

Email. Wen.wang@qmul.ac.uk

Abstract

This manuscript focuses on the movement of particles and extracellular fluid in soft tissues and microvessels. It analyses modelling applications in biological and physiological fluids at a range of different length scales: from between a few tens to several hundreds nanometers, on the endothelial glycocalyx and its effects on interactions between blood and the vessel wall; to a few micrometers, on movement of blood cells in capillaries and transcapillary exchange; to a few millimetres and centimetres, on extracellular matrix deformation and interstitial fluid movement in soft tissues. Interactions between blood cells and capillary wall are discussed when the size of the two is of the same order of magnitude, with the glycocalyx on the endothelial and red cell membranes being considered. Exchange of fluid, solutes and gases by microvessels are highlighted when capillaries have counter-current arrangements. This anatomical feature exists in a number of tissues and is the key in the renal medulla on the urinary concentrating mechanism. The paper also addresses an important phenomenon on the transport of macromolecules. Concentration polarization of hyaluronan on the synovial lining of joint cavities is presented to demonstrate how the mechanism works in principle and how model predictions agree to experimental observations quantitatively.

1. Introduction

Biofluid mechanics bridges the physical science of fluid mechanics and anatomical physiology. In the past 40 years, it has developed into an established subject of study with an increasing emphasis on multiscale events and mechanisms.[1]. Lighthill[2] classified biofluid mechanics into two categories: internal fluid mechanics and external fluid mechanics. This classification doesn't always yield simple answers when problems are examined in multiscales. For example, blood flow is commonly accepted as an internal fluid dynamics, as blood is contained inside vessels. But when we look into the interaction between blood cells and plasma, it becomes a typical external fluid problem. This is also true in soft tissue studies. Although soft tissues behave like solid material, they are more fluid-like in composition. Solid phase materials in tissues are usually interwoven into an extracellular matrix (ECM), which is constantly bathed in interstitial fluid (ISF).[3] ISF interacts with ECM and facilitates exchange with surroundings. In this paper, we highlight two aspects of transport problems: i) movement of fluid and particles in soft tissues and microvessels, and ii) exchange of fluid and solute across the vessel walls and biological membranes.

The entire vasculature, including microvessels, is lined by a monolayer of endothelial cells. On the luminal side of the endothelium, a thin layer of glycocalyx forms the interface between the circulating blood and endothelial cells.[4,5] The glycocalyx mediates the interaction between blood cells and the vessel wall,[6] affects the distribution of stresses by the circulating blood on endothelial cells,[7] and determines transcapillary exchange of fluid and solutes by controlling the permeability and solute reflection coefficient of microvessel.[8]

The major site for fluid and solute exchange between blood and surrounding tissue is in microvessels. The plasma, interstitial fluid and lymph compartments are all involved in the

continuous movement of fluid and solute in dynamic equilibrium. Due to the large number of capillaries, it is prohibitively difficult and with little scientific meaning to follow the blood flow in all capillaries in details. Symmetrical or periodic conditions and assumptions are frequently applied in studies so that a representative microcirculatory unit can be identified to provide characteristic properties of the microvascular system. In a simplified model unit, only a limited number of capillaries and neighbouring tissue are considered and exchange principles are applied.

Modelling studies should reflect tissue anatomical structures. Counter-current arrangement of microvessels is a typical feature in a number of tissues. This review summarises current understanding on this specific arrangement. Solutes considered in this review ranges from small molecules, such as oxygen or glucose that are highly permeable to capillary wall, to large molecules such as plasma proteins and macromolecules, e.g. hyaluronic acid (HA) or hyaluronan, which have limited permeability across the membrane lining and are partially reflected at the wall.[9,10] In tissues, such as the synovium of joint cavities, partial reflection of HA and high osmotic pressure associated with the elevated HA concentration, ensure normal physiological functions of the joint. Understanding of the mechanisms for fluid and solute exchange enables therapeutic strategies to be applied in treating diseases, such as HA injection in arthritic joints.

2. Interaction between blood cells and the capillary wall

It is well established that blood flow in large arteries can be described by Navier-Stokes equation, with plasma and blood cells being collectively simulated as a continuum. In microcirculation, where capillaries are comparable to red blood cells in size, such treatment is no longer valid.

Cell – vessel wall interaction in a steady parabolic flow

In microcirculation, interaction between blood cells, e.g. erythrocytes, and capillary wall has much more significant effects than that in larger vessels. Theoretical models have been built to analyse cell – wall interaction in an idealised geometry, where a sphere moves in a steady parabolic flow along a straight cylindrical tube.[11] The sphere takes arbitrary position in the tube and is free to rotate. The clearance, h defined as $R - a$, where R and a are radii of the tube and the sphere respectively, affects the choice of mathematical treatment. When R is several times bigger than a, theoretical approach using lubrication theory is no longer valid.[6] When the sphere takes eccentric positions in the tube (eccentricity, e is defined as the distance between the centre of the sphere to the axis of the tube), its motion has to be solved numerically. Figure 1 presents movements of a sphere in a microvessel with parabolic velocity profiles at the inlet and the outlet of the tube. The translating velocity decreases as the sphere moves away from the centre of the tube. As R/a increases, particularly at $R/a > 6$, the translating velocity of the sphere is increasingly dominated by the fluid velocity near its location and follows the parabolic fluid velocity more closely. The sphere's rotating velocity on the other hand increases almost linearly with e for all R/a values. The increases slow down beyond $e/c = 0.8$ and this effect is more noticeable for small sized tubes. An extension of this study has analysed the interaction between multiple particles in the microvessel. Method of fundamental solution has successfully been applied to investigate the interaction of two spheres in Oseen flows.[12]. The drag force on the leading sphere is always bigger than that on the trailing sphere, which agrees with experimental observations that blood cells in capillary tends to form columns in steady states. Another extension of the study has investigated unsteady flow conditions by employing Laplace transform.[13]

Effect of the glycocalyx on cell – wall interaction

Cells of every species are known to be covered with a dense coating of glycans.[5] Endothelial cells have a glycocalyx layer consisting of proteoglycans, glycoproteins and plasma proteins.[14] This layer has a thickness of a few tens to several hundreds nanometres and is organized into a three dimensional fibrous matrix with a regular pattern.[15] The glycocalyx a mixture of solid matrix and fluid phase and mediates interactions between blood cells and the capillary wall. Its haemodynamic effects on the cell-wall interaction have been described using a poroelastic theory.[6] The poroelastic theory is based on the continuum mechanics and mixture theory and has been widely used to study interaction between ISF and ECM in soft tissues.[16-18] Glycocalyx on the surface of the sphere and the luminal surface of the tube are represented by thin deformable porous layers. For shear flow over a porous layer, slip velocity at the interface between pure fluid and the porous layer can be derived, which relates to the velocity gradient at the interface.[19] Effects of the glycocalyx layers on movement of a sphere in a microvessel filled with an otherwise stationary fluid have been studied. It's found that the glycocalyx increases both the rotating and the translating velocities of the sphere. The ratio between the two, however, decreases, indicating a greater effect of the glycocalyx on the translating velocity than on the rotating one. Figure 2 presents the wall shear stress distribution within the lubrication zone on the surface of the tube. Due to symmetries, only a quarter of the surface area is shown. The maximum shear stress occurs where the local clearance between the sphere and the tube is the least (i.e. at $\theta = 0$), and decreases quickly towards the edge of the lubrication zone. The shear stress on the tube wall is positive at the maximum clearance and decreasing as the gap reduces to a negative minimum. By comparing results between no slip and slip conditions, it is seen that slip velocity due to the glycocalyx reduces the magnitude of shear stress on the surface of the tube.

Stress on the endothelial cell membrane mediated by the glycocalyx

When the length scale is reduced to a few tens of nanometres, one can investigate how the flow-induced stress is transmitted to and distributed on the cell membrane, as mediated by the endothelial glycocalyx. Stress by shear flow exerts on the endothelial cell membrane through two different routes: i) external shear flow induces fluid movement within the glycocalyx. If fluid movement penetrates the entire thickness of the glycocalyx, it results in a direct fluid shear stress on the membrane of the endothelium. ii) fluid drag on filaments of the glycocalyx is transmitted down to its root on the endothelial cell membrane. This stress is referred to as the 'pulling stress' on the endothelial cell membrane and will be analysed later. Structural change in the glycocalyx alters the relative contribution between the above two sources. In Figure 3, we present a simple case of steady laminar flow in a vessel lined with a layer (thickness = ε) of glycocalyx. The shear stress at the fluid-glycocalyx interface $r = R$ can be easily derived as $\tau_0 = -\frac{GR}{2}$, where G is the axial pressure gradient in the vessel. The fluid velocity within the glycocalyx can be solved from the poroelastic theory. The 'pulling stress', τ, on the cell membrane caused by the fluid drag on fibrils of the glycocalyx is derived as follows,

$$\frac{\tau}{\tau_0} = (1-\phi)\left\{1+\phi\left[1-\cosh^{-1}(\alpha)+\frac{2\varepsilon}{R}\left(1-\frac{\tanh(\alpha)}{\alpha}\right)\right]\right\}, \qquad (1)$$

where $\alpha = \sqrt{k/\mu_a\varepsilon}$ is an intermediate parameter and ϕ is the porosity of the glycocalyx (see Ref. 7 for details). Fluid velocity in the vessel (both inside and outside the glycocalyx layer) is presented in Figure 3a. In the pure fluid region, parabolic velocity profile is seen with the peak velocity at the centre of the tube. Within the glycocalyx layer, fluid velocity decreases from the interface to zero at the wall. In Figure 3b, the pulling stress on the cell membrane (τ/τ_0) is presented, as is the effect of changes in the glycocalyx structure on the magnitude of the pulling stress. When degeneration of the endothelial glycocalyx occurs under oxidative

stress or enzymatic treatment, ϕ increases and α decreases at the same time. Contribution to the membrane stress via pulling of the matrix filaments of the glycocalyx is seen to decrease significantly. Concomitantly, fluid movement within the glycocalyx induces a higher shear rate on the cell membrane, compensating for the reduction in the solid pulling stress. The accompanying reduction in the height of glycocalyx layer during degeneration (as indicated in dashed curves) will further exacerbate this effect. The results give insight to the glycocalyx mediated stress distribution on endothelial cell membrane.

3. Interaction between the interstitial fluid and extracellular matrix

Most soft tissues resemble glycocalyx in composition. They consist of ISF mainly made of water and dissolved solutes and ECM made of collagen and proteoglycans. Their composition equilibrium during homeostasis is regulated by residing cells. ISF and ECM interact with each other and cooperate to perform soft tissue's specific functions. When tissue degenerates under abnormal conditions, this interaction is disrupted and its function impaired. Poroelastic theory is used to describe the mechanical response of soft tissues, taking account of their multiphasic feature. Finite element simulation is conducted to study the ECM-ISF interaction in a generic soft tissue under cyclic loadings in a new loading configuration – confined indentation. As shown in Figure 4, a dynamic loading of frequency f = 0.1 Hz is applied to the top central boundary. In the loading phase, a high interstitial fluid pressure develops in the central region of sample corresponding to local compression. As a result, fluid is squeezed out. In the unloading phase, the central region becomes depressurized as ECM compression is released. Fluid will be re-imbibed back to the low pressure region. This active pressure zone just beneath the indenter is the key to the extraordinary load bearing performance of the articular cartilage as the loading configuration is more representative of physiological loading conditions of the articular cartilage in joints than others. Mechanical

responses are transmitted to residing cells which in turn regulate cell activities. Poroelastic theory has been used to describe chondrocytes and articular cartilage in multi-scale models.[20] Under a static loading, stress concentration at the cell-matrix border is observed due to large difference in mechanical properties of cells and ECM. Consideration of pericellular matrix – a thin layer adjacently enclosing the chondrocyte – significantly alters the stress and strain magnitudes within the chondrocytes, suggesting a functional biomechanical role. Furthermore, fluid circulation between central and peripheral regions assists the solute transport in the avascular tissue. When consumption and production of a specific solute is considered simultaneously with solute diffusion and convection, enhanced solute transport is observed for a range of solutes under the dynamic loading.[21] This is in line with the symmetry-breaking mechanisms proposed by Gardiner et al.[22]

4. Transcapillary exchange of fluid and solute in the microcirculation

Solute transport between vascular vessels and exravascular tissue is very important to nutrient supply and waste product removal. The capillary bed is the main site for these exchanges, where the number and the surface area of capillaries are high and the blood flow velocity is low. Fluid exchange in most tissues can be described by the Starling principle that the fluid flow across the vessel wall is driven by the hydrostatic pressure and osmotic pressure differences between the lumen and the interstitium,[23,24]

$$J_v = PA\left(\Delta p - \sigma \Delta \Pi\right) \qquad (2)$$

where J_v is the volume filtration rate per unit area, Δp is the difference in hydrostatic pressure, σ is the molecule reflection coefficient and ΔΠ is the difference in osmotic pressure across the vessel. This review selects a number of tissues with unique microvascular arrangements to illustrate the exchange mechanism for fluid and solutes.

Oxygen transport in outer layers of the skin

In the cutaneous microcirculation, as shown in Figure 5a), the arterial supply and venous drainage for the skin are located deep in the hypodermis. Two important plexuses are found in the dermis: the deeper one at the junction of the hypodermis and the dermis and the superficial sub-papillary one just beneath the dermal papillae.[25] The sub-papillary plexus forms a capillary loop in each papilla and nutritions the upper layer of the dermis. Oxygen partial pressure (pO_2) distribution in epidermis, dermis and hypodermis in human nail folds has been measured using oxygen sensitive microelectrodes.[26] In order to establish detailed distribution of oxygen partial pressure, a three dimensional cubic microcirculatory model unit was set up and oxygen distribution was solved for numerically.[27] The model was composed of the epidermis, germinal layer and dermis with the underlying sub-papillary plexus and an associated capillary loop located on the symmetrical-plane. Oxygen distribution is governed by the diffusion-consumption equation in each layer

$$\alpha \frac{\partial p}{\partial t} = D\alpha \nabla^2 p - mH + S\,, \qquad (3)$$

where D is the oxygen diffusion coefficient, α the oxygen solubility coefficient, m the oxygen consumption rate and S the oxygen supply rate from blood. While in capillary the convection transport and diffusion loss across the capillary wall dictates its distribution

$$A\frac{\partial C_v}{\partial t} + Q\frac{\partial C_v}{s} = -q(s)\,, \qquad (4)$$

where C_v is the oxygen concentration in the blood, A is the cross sectional area of the papillary loop and Q is the capillary flow rate. $q(s)$ is the trans-capillary oxygen flux caused by diffusion of the oxygen between the blood and the tissue. Figure 6 b and c show the steady state oxygen distribution in the symmetric-plane when the blood perfusion rate in the papillary loop is Q = 10^{-8} ml/s. When the skin is in direct contact with the air (i.e. at 160 mmHg) in Figure 6b, oxygen is supplied from both the sub-papillary plexus and the

atmosphere through the epidermis. As a result, high pO_2 values are observed in both hypodermis and epidermis, which gradually decrease towards the middle region the dermis due to active cellular consumption there. The lowest value is observed in the periphery region of germinal layer. When the skin is covered by an oxygen-free medium, the sub-papillary plexus becomes the only source of oxygen supply, which results in a monotonically decrease in pO_2 from the hypodermis to the epidermis. In some outermost region of epidermis, cells become starved of oxygen. If the situation persists, local cells will no longer be viable. The model study makes it possible to evaluate detailed contribution of oxygen from each source to meet skin metabolic requirement.

Inert gas clearance from the tissue

Inert gases are not involved directly in cellular metabolism and their transport problem has largely been overlooked. In a number of situations, understanding of the inert gas transport is very important, for example in air decompression sickness and in anaesthesia control.[28] Making use of its inert nature, isotope-labelled inert gas has been used to determine tissue perfusion – an important but extremely difficult task for direct measurement. A compartment model is commonly used to interpret measurement data, which assumes instantaneous mixing of the inert gas in tissue and capillary compartments.[29] Although this simplification brings mathematical convenience, omitting radial and longitudinal gradients of the inert gas limits its application, particularly in relatively poorly-vascularised tissues, where diffusive transport of the gas is comparable to the convective one. A three dimensional model has been developed to investigate inert gas diffusion and convection in a representative microcirculatory unit, enclosing either a single capillary or multiple capillaries. We are particularly interested in two-capillary systems, where flow is either co-current or counter-current. Figure 6a presents simulated inert gas distribution in the tissue after a period of

clearance. Initially, inert gas saturates both the capillary and the surrounding tissue. Its partial pressure decreases following the perfusion with the inert gas-free blood. In the single capillary model, blood flow results in a unidirectional gradient of the inert gas along the flow direction, with the lower value at the inlet end. A similar distribution pattern, but of much lower partial pressure of the inert gas, is observed in the co-current model, in which the total flow rate is doubled (two capillaries ca. single capillary with same flow rate in all vessels). On the other hand, the counter-current arrangement of capillaries (with the same total perfusion rate), has a much less capacity for the inert gas clearance. High concentration inert gas is trapped in the centre of the unit, although the clearance takes place near both ends of the unit. This is caused by the cross sectional diffusion between the current-current capillaries that retards the inert gas clearance from the outlets. Figure 6b highlights the potential problem in determining the blood perfusion rate using the inert gas clearance method according to above numerical simulation. The exact experimental procedure is followed to estimate the blood perfusion rate based on the gas clearance rate.[29] The estimated value is plotted against the actual blood flow rate used in the model. As shown in the figure, if tissues only have single or co-currently arranged capillaries, then the method based on the inert gas clearance gives reasonable estimation of the actual blood perfusion rate. In tissues with counter-currently arranged microvessels, the inert gas clearance method only provides rough estimation at low perfusion rates. However the actual perfusion is significantly underestimated at middle or high perfusion rates. As counter-current arrangement of microvessels is common in a number of tissues, for example the liver and kidney, extra caution should be exercised in using inert gas clearance method to estimate tissue perfusion rate of those tissues.

Counter-current exchange in renal medulla

For small solutes, such as Na^+, K^+ and urea, similar 'diffusive trapping' between counter-currently arranged capillaries can is also expected. Intensive counter-current exchange vessels exist in the renal medulla. One well known example is loops of Henle, which is responsible for urinary concentration process.[30,31]. Descending vasa recta (DVR) and ascending vasa recta (AVR) form another counter-current loop that runs in parallel to the loops of Henle. Counter-current exchange between DVR and AVR has been studied on its role in preserving high concentration of small solute in ISF.[32] Under physiological conditions in the renal medulla, the counter-current arrangement of vasa recta serves to preserve a higher gradient of solute concentration in the interstitium. In addition, variation in blood flow rate has a much more pronounced effect on solute concentration gradient with counter-current capillary arrangement than with a single capillary. When anti-diuretic hormone reduces medullary blood flow, the counter-current arrangement of vasa recta favours a much more rapid accumulation of solutes in the ISF. When other physiological features are considered, such as the existence of anastomoses between DVR and AVR and change of both the flow rate and the average cross-sectional area of vasa recta with the distance, an exponential increase is predicted in corticomedullary solute concentration (Figure 7), which agrees with results from electron probe measurement.[33]

Plasma proteins and their associated oncotic pressure play an important role in fluid exchange between blood and the interstitial fluid. In normal tissues, proteins that are leaked out from capillaries are reabsorbed by lymphatic microvessels nearby. In the inner medulla of the kidney, there is no evidence for lymphatic vessels, as yet both DVR and AVR are permeable to albumin. It has long been speculated that the most likely route for the removal of the plasma protein that leaks out of the DVR is through the convective re-absorption into the AVR.[34] Emerging experimental evidence on difference properties of AVR and DVR supports

this speculation. This hypothesis has been tested using the above-mentioned counter-current exchange model. For the hypothesis to work, there are a number of known facts that the model predictions have to satisfy: albumin concentration in the ISF is significantly lower than that in DVR and AVR, the unit as a whole shall have the capacity for net re-absorption of water from the nephron, an increase in flow rate in vasa recta shall result in lower albumin concentration in the ISF and higher water re-absorption capacity of the unit. Wang and Michel[35] demonstrated in their model study that albumin convection into the AVR could function in principle. Their model predictions agree to all known fluid and albumin distribution features in the renal medulla, supporting the hypothesis that leakage of plasma proteins from the DVR into the ISF is balanced, in the absence of lymph microcirculation in the inner medulla, by clearance into the AVR.[35] Modeling of solute transport and fluid exchange in renal medulla becomes more and more complicated when more physiological and anatomical features are disclosed. Aquaporin is found to exist in the DVR, which provide an exclusive channel to the water. This channel is generally regarded as impermeable to all other solutes thus even small solutes will exert an osmotic pressure on the water exchange. This effect is considered in a numerical model where aquaporin-1 is found to maintain the high osmolarity in the renal papillary region, which is abolished when aquaporin channels are depleted.[36] The findings of other specialized features such as urea transporter will induce more complicated process. Furthermore, no-one has tried to link the outer-medullar transport and inner-medullar transport although they are an integral part of the renal concentrating mechanisms. All these require the development of a more sophisticated multiscale model.

5. Transport of hyaluronan across the synovial lining of joint cavities

Synovial fluid is an ultrafiltrate of blood plasma and is made very viscous by addition of a macromolecule, hyaluronic acid (HA, or hyaluronan), which is secreted by B-type

synovicytes in the synovial lining. When joint is under loading, such as in joint flexion, synovial fluid will permeate the synovial lining and drain into lymphatic vessels in the subsynovium. Fluid preservation in pressurised joint is essential for the normal function of synovial joints. Hyaluronan has been known as an important lubricant in joint motion.[37] Recently its new role in preserving synovial fluid was investigated.[38] Experimental evidence has revealed that when synovial fluid is depleted of HA, increasing intra-articular pressure results in significant increase in trans-synovial fluid flow. However, the presence of HA dramatically reduces the outflow which is made nearly insensitive to increases in intra-articular pressure once pressure is above a certain value. Due to its large radius of gyration, HA molecule's reflection coefficient at the synovial lining is more than 0.6. It has been hypothesized that osmotic pressure due to increased HA concentration at the synovial lining counter-balances the elevated intra-articular pressure.[38]. Recent studies have put this hypothesis to test, quantitatively, by using a non-steady state dead-end model and by following the exact experimental protocol step-by-step.[39,40] The model employs a simple convection-diffusion equation and is based on mass and volume conservation of HA and synovial fluid. The validity of such model is justified by a satisfactory agreement between experimental data and numerical prediction found for a sequential change in the intra-articular pressure for a range of perfusate concentrations (Figure 8a). Numerical modelling for the first time predicts the development of concentration polarization layer, most of which takes 3 hours (experimental time) to develop but complete formation takes much longer time. The calculated osmotic pressure based on the predicted HA concentration on the synovial lining offers a reasonable and quantitative explanation for the puzzled HA trans-synovial flow buffering phenomena: HA molecules accumulated on the synovial lining and resultant high concentration osmotically counteract the increase of intra-articular pressure, buffering the trans-synovial flow even joint is in unfavourable high pressure condition.

5. Summary and future perspective

Interaction between fluid and biological cells is an interesting but challenging problem in biofluid mechanics. This is particularly so in the microvascular system, where interactions between plasma, blood cells and capillary wall need to be considered. Although some full numerical approaches have the potential to mimic fluid-cell interactions under simplified conditions, their value is yet limited in advancing our understanding of problems such as cell rolling and adhesion on the vascular endothelium.[41] The presence of the glycocalyx on endothelial and red blood cells introduces another element of complexity in fluid-cell and cell-cell interactions. Fluid exchange in the microvascular bed is governed by the Starling's principle. Solute transport depends on solute diffusion and its convection by the blood circulation. Transcapillary exchange of the solute is determined by the permeability of the capillary to the solute. For large sized molecules, their reflection at the wall usually leads to the build-up of a concentration polarization layer, which can play a significant role in altering fluid exchange via resultant osmotic pressure. Counter-current exchange arrangement is a common feature in physiological systems. In comparison to co-current capillary arrangement, it has a more intriguing effect on solute supply to and clearance from tissues. The discovery of the endothelial glycocalyx was a significant event in vascular physiology. In addition to its role in endothelial mechanotransduction, the presence of the endothelial glycocalyx challenges us to reconsider the conventional Starling principle for transcapillary fluid exchange.[24]

Biofluid mechanics has wide applications in biomedical sciences: from large vessel haemodynamics to cell and tissue engineering. In microcirculation, Reynolds number is typically low. This makes possible certain asymptotic approaches in micorvascular haemodynamics. In applying fluid mechanical principles, simplification is frequently adopted

to render complex problems amenable to theoretical or numerical consideration. The challenge is to achieve this without losing main features of the physiological problem. In the study of the endothelial glycocalyx, poroelastic theory has been applied and gives a number of useful insights into its role on velocity and wall stress distribution. However, the current model for the glycocalyx is far from satisfactory. For example, the glycocalyx has strong negative fixed charges, which will endow the matrix a stronger resistance to deformation than usually anticipated. The impact of the negative charges on the mediation of shear stress exertion and solute transport remains an enigma. Due to the interdisciplinary nature of the subject, it is essential to have effective communication between fluid mechanists and physiologists. Theoretical analysis and numerical models need to be based on experimental observations and serve to gain new insights into physiological problems.

References

1. Y. C. Fung, *Biomechanics: Circulation* (Springer-Verlag, NY, 1984).
2. J. Lighthill, *Mathematical Biofluiddynamics* (Society for Industrial and Applied Mathematics, Philadelphia, 1975).
3. M. A. Swartz and M. E. Fleury, Intersitial flow and its effects in soft tissues, *Annu. Rev. Biomed. Eng.* **9** (2007) 229-256.
4. A. Silberberg A, Polyelectrolytes at the endothelial cell surface, *Biophys. Chem.* **41** (1991) 9-13.
5. A. Varki Glycan-based interactions involving vertebrate sialic-acid-recognizing proteins, *Nature* **446** (2007) 1023–1029.
6. W. Wang and K. H. Parker, The effect of deformable porous surface layers on the motion of a sphere in a narrow cylindrical tube, *J. Fluid Mech.* **283** (1995) 287-305.
7. W. Wang, Change in properties of the glycocalyx affects the shear rate and stress distribution on endothelial cells, *J. Biomech. Eng.* **129** (2007) 324-329.
8. B. M. Fu, S. Weibaum, R. Y. Tsay and F. E. Curry, A junction-orifice-fiber entrance layer model for capillary permeability: application to frog mesenteric capillaries, *J. Biomech. Eng.* **116** (1994) 502-513.
9. K. H. Parker and C. P. Winlove, The macromolecular basis of the hydraulic conductivity of the arterial wall, *Biorheology* **21** (1984) 181-196.
10. W. Zhang and C. R. Either, Direct pressure measurements in a hyaluronan ultrafiltration concentration polarization layer, *Colloids Surf. A* 180 (2001) 63-73.
11. P. H. Wen, M. H. Aliabadi and W. Wang, Movement of a spherical cell in capillaries using a boundary element method, *J. Biomech.* **40** (2007) 1786-1793.
12. W. Wang and P. H. Wen, Interaction between micro-particles in Oseen flows by the method of fundamental solutions, *Eng. Anal. Bound. Elem.* **32** (2008) 318-327.
13. P. H. Wen, Y. C. Hon and W. Wang, Dynamic responses of shear flows over a deformable porous surface layer in a cylindrical tube, *Appl. Math. Model*. **33** (2009) 423-436.
14. J. H. Luft, Fine structure of capillary and endocapillary layer as revealed by ruthenium red, *Fed. Proc.* **25** (1966). 1773-1783.
15. J. M. Squire, M. Chew, G. Nneji, C. Neal, J. Barry and C. C. Michel, Quasi-periodic substructure in the microvessel endothelial glycocalyx: a possible explanation for molecular filtering?, *J. Struct. Biol.* **136** (2001) 239-255.

16. R. M. Bowen, Incompressible porous media models by the theory of mixture, *Intl. J. Engng. Sci.* **18** (1980) 1129-1148.
17. V. C. Mow, M. H. Holmes and W. M. Lai, Fluid transport and mechanical properties of articular cartilage: a review, *J. Biomech.* **17** (1984) 377-394.
18. Y. Lu and W. Wang, Interaction between the interstitial fluid and the extracellular matrix in confined indentation, *J. Biomech. Eng.* **130** (2008) 041011.
19. J. S. Hou, M. H. Holmes, W. M. Lai and V. C. Mow, Boundary conditions at the cartilage-synovial fluid interface for joint lubrication and theoretical verifications, *J. Biomech. Eng.* **111** (1989) 78-87.
20. F. Guilak and V. C. Mow, The mechanical environment of the chondrocyte: a biphasic finite element model of cell-matrix interactions in articular cartilage, *J. Biomech.* **33** (2000) 1663-1673.
21. Y. Lu and W. Wang, Solute transport in porous medium under external loads. *Proc. ASME Heat Transfer/Fluids Eng.* HT-FED04-56159 (2004), pp. 1-4
22. B. Gardiner, D. Smith, P. Pivonka, A. Grodzinsky, E. Frank and L Zhang, Solute transport in cartilage undergoing cyclic deformation, *Comp. Methods Biomech. Biomed. Eng.* **10** (2007) 265-278.
23. C. C. Michel and F. E. Curry, Microvascular permeability, *Physiol. Rev.* **79** (1999) 703-761
24. J. R. Levick and C. C. Michel, Microvascular fluid exchange and the revised Starling principle, Cardiovas. Res. (2010) DOI:10.1093/cvr/cvq062.
25. I. M. Braverman, The cutaneous microcirculation: ultrastructure and microanatomical organization, *Microcirculation* **4** (1997) 329-340.
26. W. Wang, C. P. Winlove and C. C. Michel, Oxygen partial pressure in outer layers of skin of human finger nail folds, *J. Physiol.* **549** (2003) 855-863.
27. W. Wang, Oxygen partial pressure in outer layers of skin: simulation using three-dimensional multilayered models, *Microcirculation* **12** (2005) 195-207.
28. B. A. Hills, Vital issues in computing decompression schedules from fundamentals II. Diffusion versus blood perfusion in controlling blood: tissue exchange, *Int. J. Biometeorol.* **14** (1970) 323-342.
29. N. A. Lassen, O. Henriksen and P. Sejrsen P, Indicator methods for measurement of organ and tissue blood flow, *Handbook of Physiology (Sec 2): The Cardiovascular System, Vol III*, eds J. T. Shepherd and F. M. Abboud (Am Physiol Soc, Bethesda, 1983), pp. 21-63

30. T. L. Pallone, C. R. Robertson and R. L. Jamison, The renal medullary microcirculation, *Physiol. Rev.* **70** (1990) 885-920.
31. T. L. Pallone, M. R. Turner, A. Edwards and R. L. Jamison. Counter-current exchange in the renal medulla, *Am. J. Physiol. Regul. Integr. Comp. Physiol.* **284** (2003) 1153-1175.
32. W. Wang and C. C. Michel, Effects of anastomoses on solute transcapillary exchange in countercurrent systems, *Microcirculation* **4** (1997) 381-390.
33. J. P. Koepsell, W. A. P. Nicholson, W. Kriz and H. J. Hohling, Measurements of exponential gradients of sodium and chlorine in the rat kidney medulla using the electron microprobe, *Pflugers Arch.* **350** (1974) 167-184.
34. C. C. Michel, Renal medullary microcirculation: architecture and exchange, *Microcirculation* **2** (1995) 125-139.
35. Wang W and Michel CC (2000) Modeling exchange of plasma proteins between microcirculation and interstitium of the renal medulla, *Am. J. Physiol. Renal Physiol.* **279** (2000) 334-344.
36. T. L. Pallone, A. Edwards, T. Ma, E. P. Silldorff and A. S. Verkman, Requirement of aquaporin-1 for NaCl-driven water transport across descending vasa recta, *J. Clin. Invest.* **105** (2000) 215-222.
37. B. J. Roberts, A. Unsworth and N. Mian, Models of lubrication in human hip joint, *Ann. Rheum. Dis.* **41** (1982) 217-224.
38. P. J. Coleman, D. Scott, R. M. Mason and J. R. Levick, Characterization of the effect of high molecular weight hyaluronan on trans-synovial flow in rabbit knees, *J.Physiol.* **514** (1999) 265-282.
39. Y. Lu, J. R. Levick and W. Wang, Concentration polarization of hyaluronan on the surface of the synovial lining of infused joints, *J. Physiol.* **561** (2004) 559-573.
40. Y. Lu, J. R. Levick and W. Wang, The mechanism of synovial fluid retention in pressurized joint cavities, *Microcirculation* **12** (2005) 581-595.
41. S. Li and W. K. Liu, *Meshfree Particle Methods* (Springer Berlin Heidelberg, 2004).

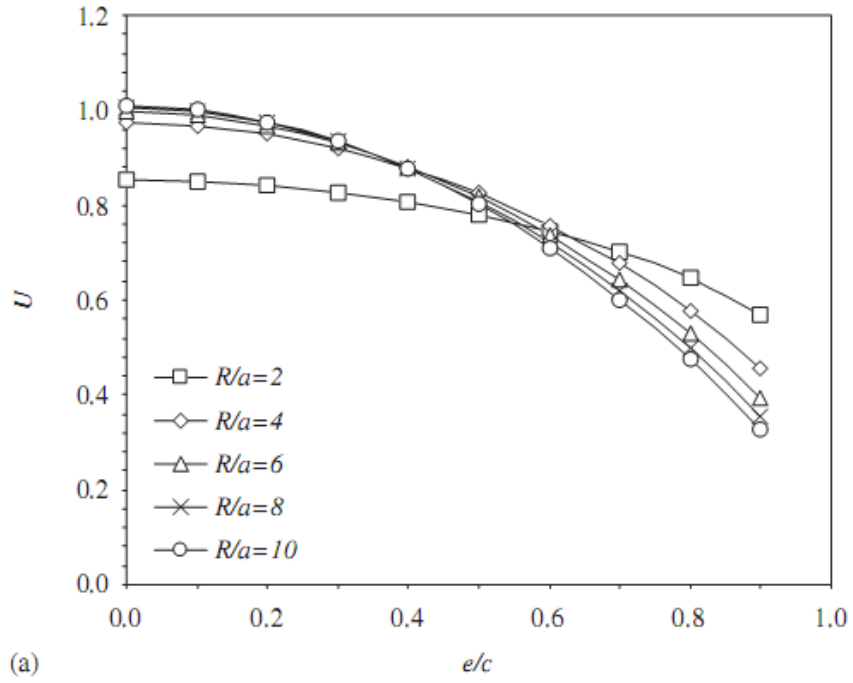

(a)

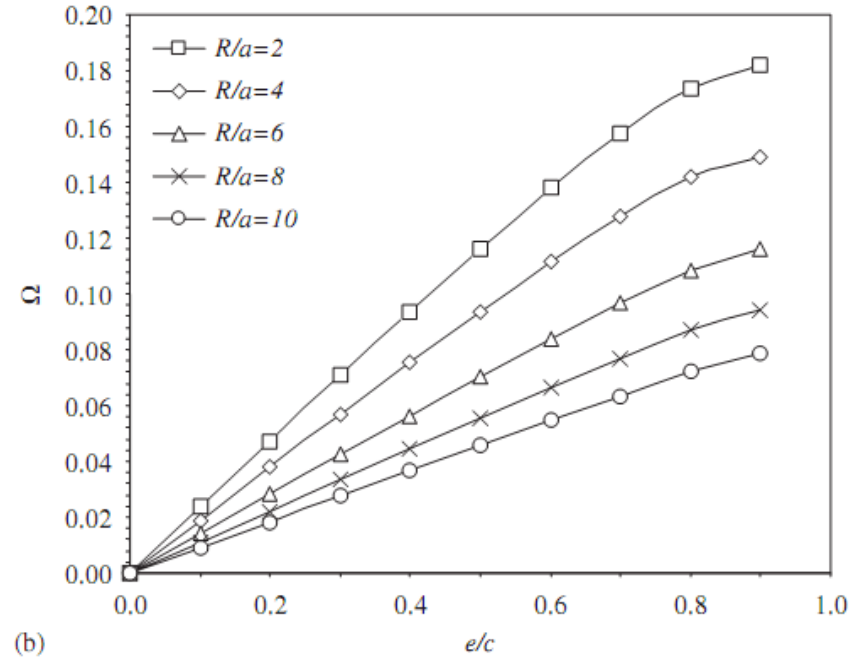

(b)

Figure 1. Translating (panel a) and rotating (panel b) velocities of a sphere in a micro-tube with a parabolic flow imposed at its inlet and outlet. Reproduced from Wen *et al*., 2007.

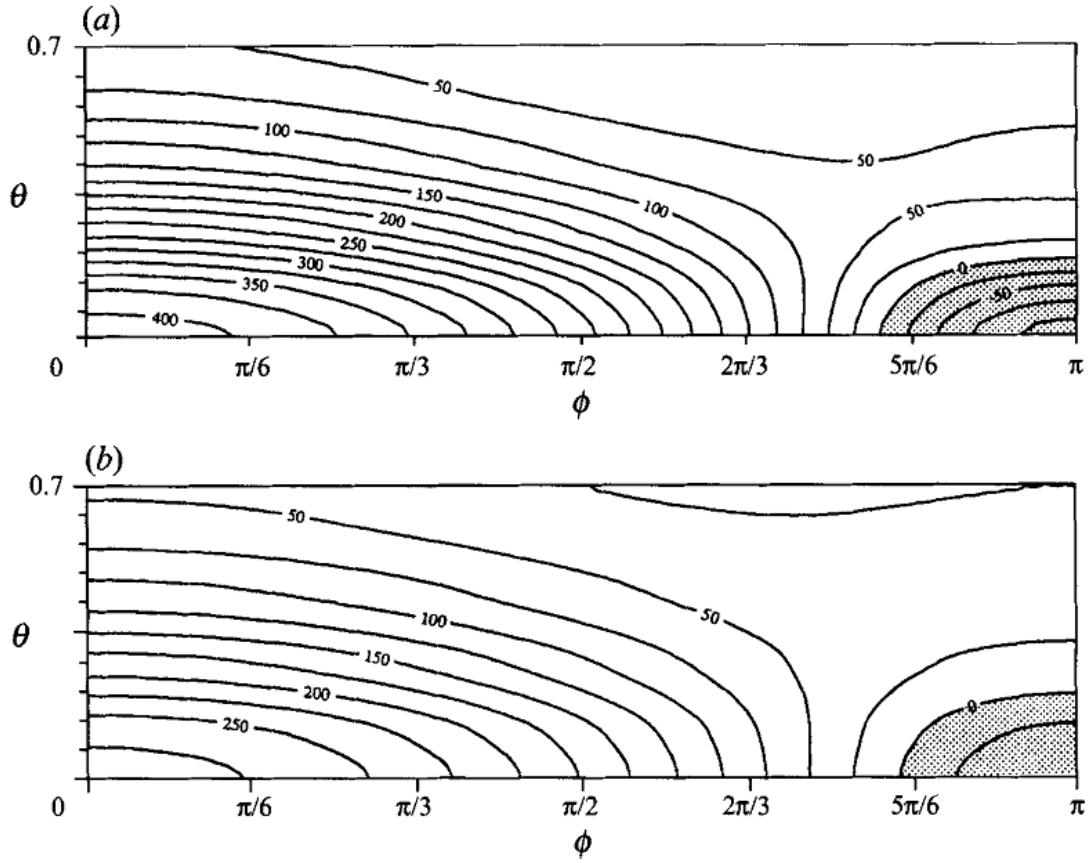

Figure 2. Shear stress contours on the surfaces of the tube under different boundary conditions. (a) with the no-slip condition on the walls, and (b) with slip boundary condition that represents effects of the glycocalyx layer. ϕ and θ represent the angular coordinate. Details can be found in Wang & Parker, 1995.

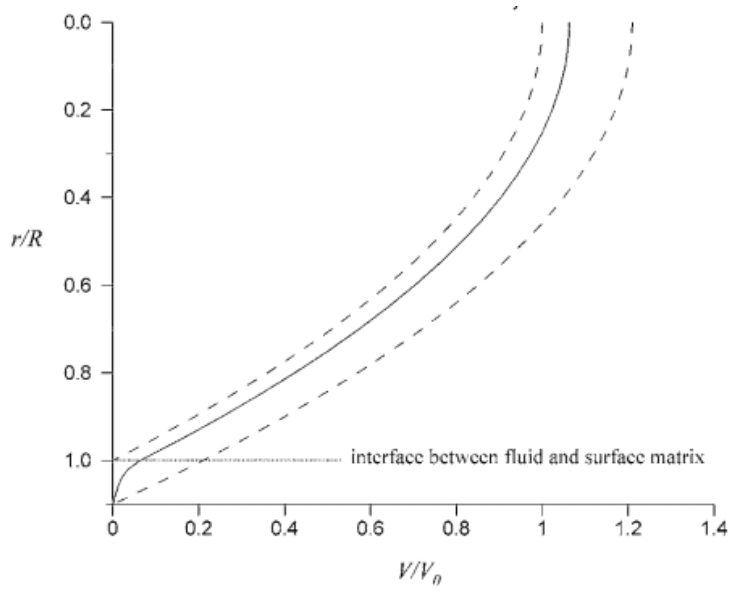

a)

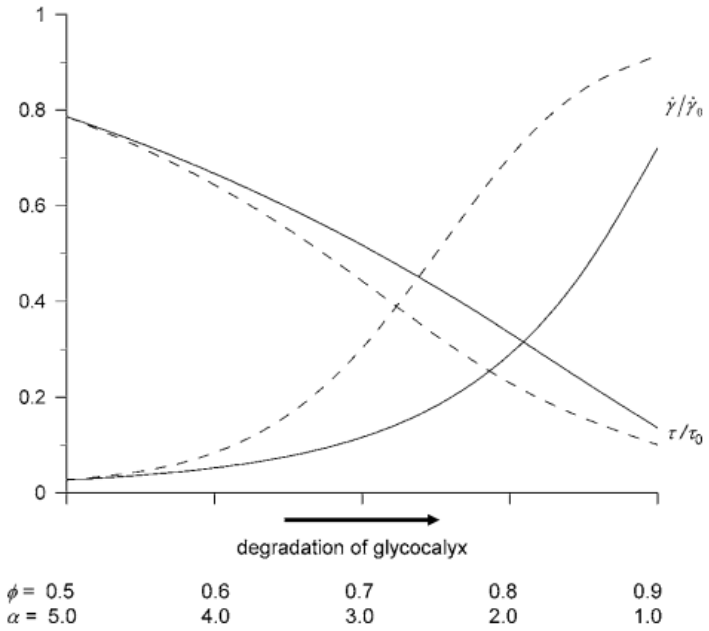

b)

Figure 3. a) Fluid velocity profile in the lumen of the vessel. ε/R = 0.1, ϕ = 0.9 and α = 3.0. The two dashed lines represent limiting cases when ϕ = 0 and 1. b) Changes in 'pulling stress' and shear rate on the vessel wall following structural change in the glycocalyx layer. Dashed lines represent the change of stress after incorporation of accompanying change in the thickness of the glycocalyx layer. Adapted from Wang, 2007.

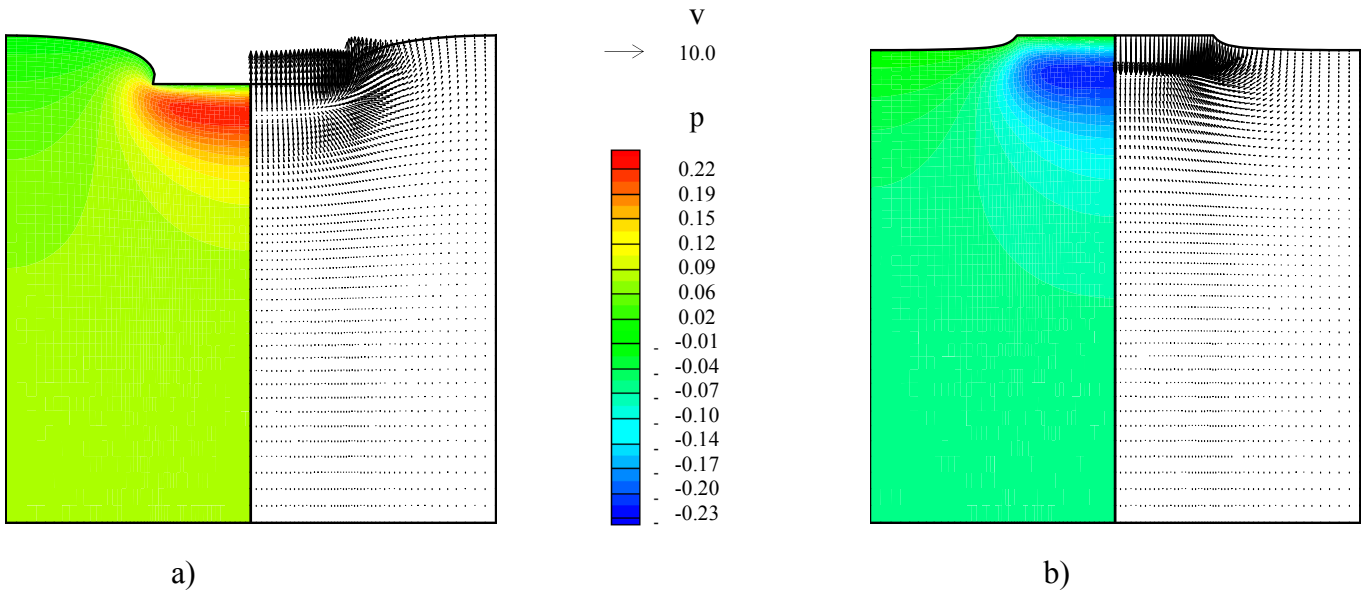

Figure 4. Mechanical response of a cylindrical soft tissue in the confined indentation configuration. Soft tissue is dynamically loaded at a frequency 0.1 Hz in the top central boundary. a) soft tissue is under the maximum compression, b) soft tissue is subjected to zero compression. The left panel and right panel of each figure plot the interstitial fluid pressurization and fluid movement at the same time on the same cross section. Adapted from Lu & Wang 2008.

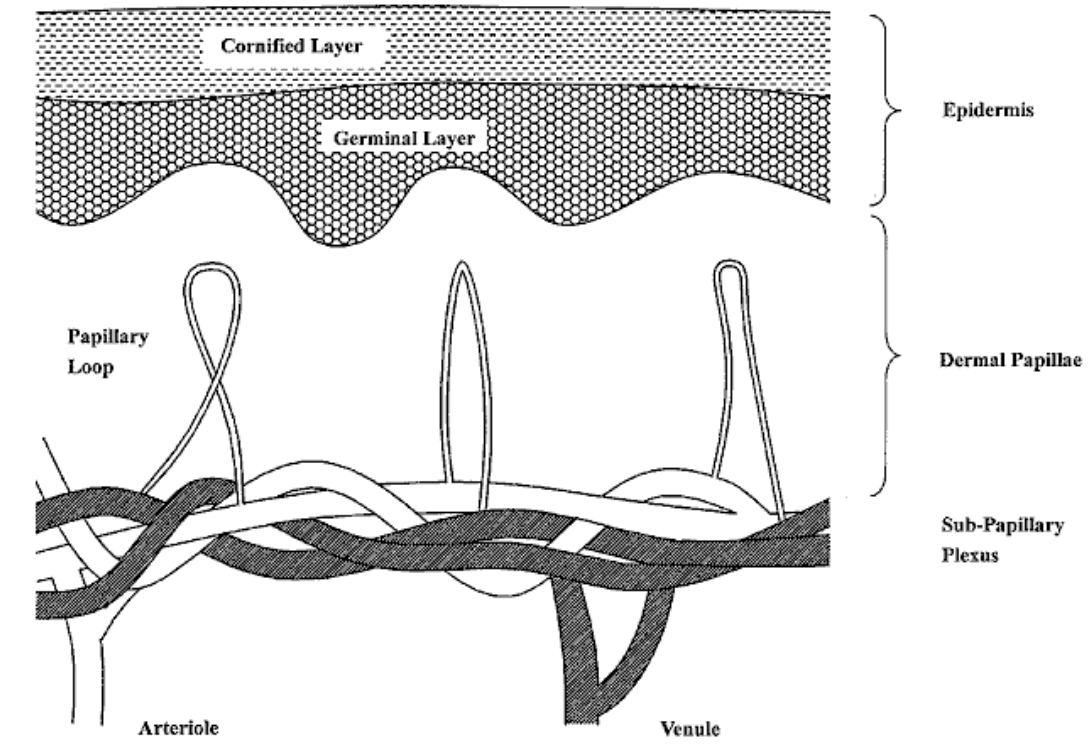

a)

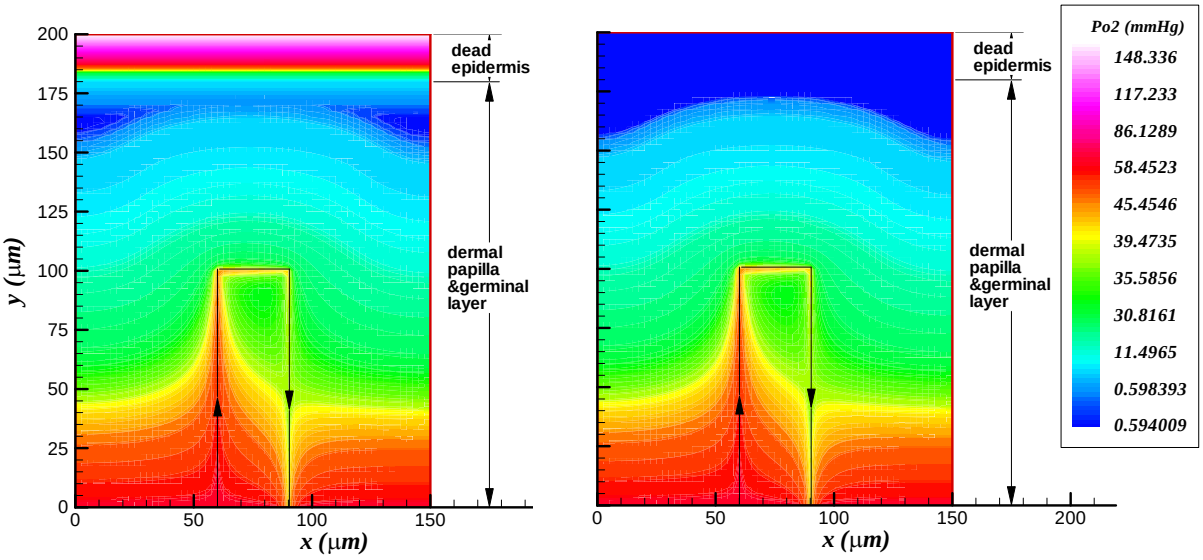

b)

Figure 5. a) Schematic drawing of the anatomical structure of superficial layers of the skin. From the bottom, the subpapillary plexus, dermal papillae including papillary loops, the germinal layer, and the cornified stratum corneum are shown. b) pO2 distribution in the symmetrical plane of a three dimensional microcirculatory unit under two different conditions: skin is in direct contact with air (left panel), and skin is cover by an oxygen-free medium (right panel). Adapted from Wang, 2005.

a)

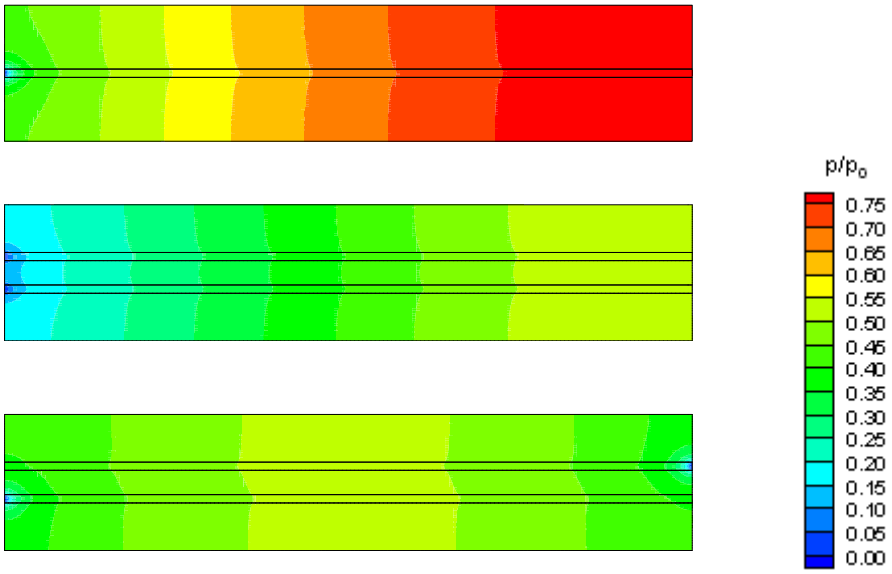

b)

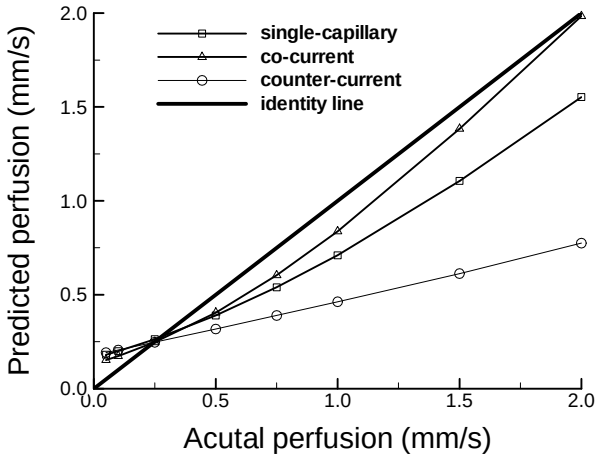

Figure 6. Pressure contours of the inert gas following the perfusion of the initially gas saturated tissue (radius = 50 μm and length = 500 μm) with gas-free blood at t = 160 seconds. Microvessels are all of the same size (radius = 3 μm) and have the same blood flow (0.5 mm/sec). Gas diffusivity is 1.0×10^{-5} cm^2/s and 0.5×10^{-5} cm^2/s respectively in the blood and the tissue. Gas solubility in the tissue is twice that in the blood.
a) Contours of the gas partial pressure in capillaries and tissues. Top, with a single capillary; middle with a co-current capillary pair; Bottom, with a counter-current capillary pair.
b) Predicted tissue blood perfusion velocity vs. actual perfusion velocity for different microvascular arrangements over a physiological range of values for perfusion.

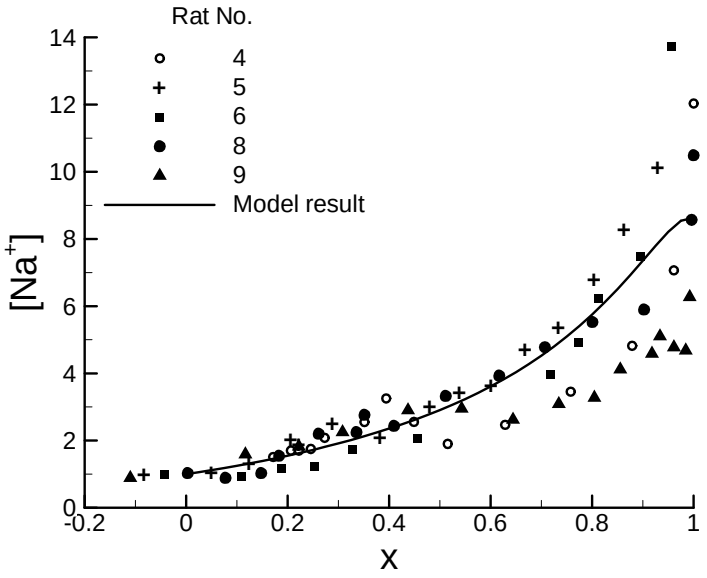

Figure 7. Comparison between the model prediction and animal experimental results on Na^+ concentration in the ISF. Reproduced from Wang & Michel, 1997.

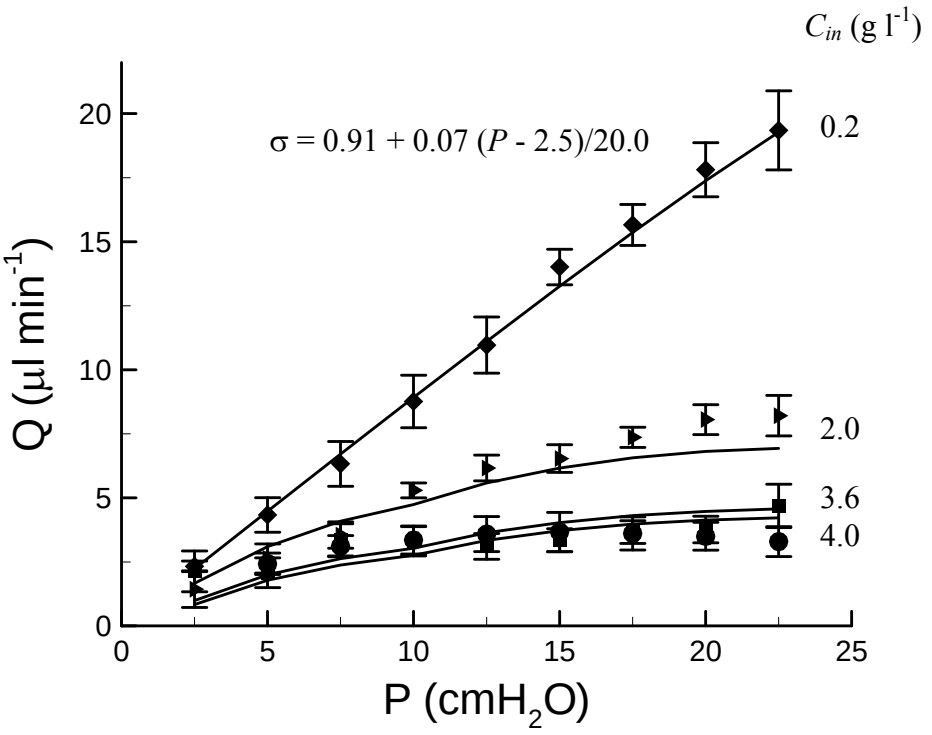

a)

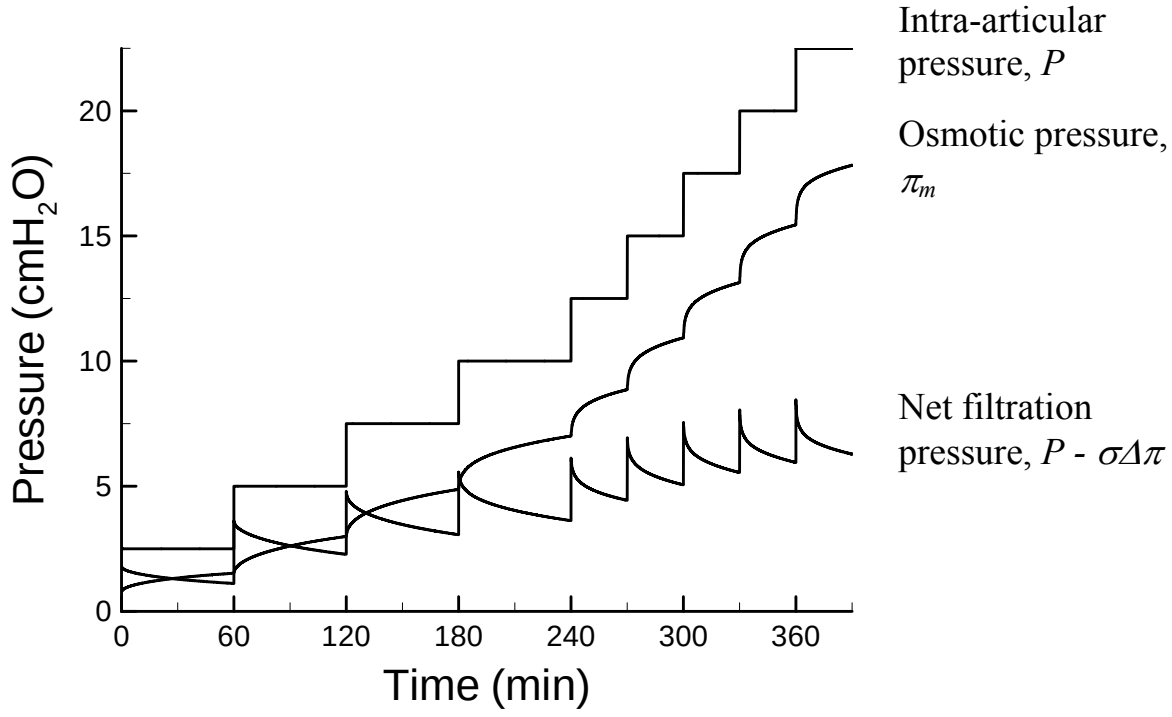

b)

Figure 8. a). Comparison of theoretical predictions (curves) with experimental measurements of effect of intra-articular pressure P on trans-synovial fluid Q in the presence of infused HA of concentration C_{in} = 0.2, 2.0, 3.6 and 4.0 g l^{-1}; b). Computed changes in the filtration pressures P, π_m and $[P - \sigma\Delta\pi]$ during a continuous infusion of 3.6 g l^{-1} of HA into a rabbit knee during timed, sequential steps rises in P. Adapted from Lu et al., 2005.